K. Dohan* and B. R. Sutherland
University of Alberta, Edmonton, Canada

1. INTRODUCTION

Turbulent regions adjacent to stably stratified regions in which internal waves may propagate are a common occurrence in geophysical flows, as in the oceanic boundary layer overlying the seasonal thermocline.

High turbulent dissipation rates are observed in the ocean interior over mid-ocean ridges and are most likely attributed to breaking internal waves generated by tidal flows over the topography. The turbulence created by the rubbing of tidal currents over the rough topography may be an additional internal wave source, and may contribute to the high dissipation rates.

However, the generation of waves from turbulence is poorly understood and the properties of these waves are unknown.

This investigation uses salt water tank experiments to measure the properties of internal waves that are generated below an idealized layer of turbulence, in the first laboratory study of the problem (Dohan and Sutherland 2003). Numerical simulations are performed to further examine the generation of internal waves from a mixed region.

2. EXPERIMENTAL SET-UP

Experiments are performed in an acrylic tank of horizontal dimensions $W = 9.7\text{cm}$, $L = 47.6\text{cm}$ and of height $H = 49\,\text{cm}$, as shown in Figure 1. This geometry allows us to record wave motions that are quasi-two-dimensional (in the $x-z$ plane).

The tank is initially filled tank with uniformly salt-stratified water. The strength of the stratification may be represented by the (initially constant) buoyancy frequency, N, which ranges between $0.33\,\text{s}^{-1}$ and $1.40\,\text{s}^{-1}$. A stainless steel mixer is inserted at the top of the tank. The mixer is a ladder-shaped grid of hollow cylindrical bars of diameter 0.6 cm spaced 3.2 cm apart. When switched on, the mixer moves vertically with a frequency of 7 Hz and with a peak-to-peak stroke length of 2.6 cm.

*Corresponding author: Dept. of Mathematical and Statistical Sciences, U. Alberta, Edmonton, AB T6G 2G1, Canada; e-mail: dohan@math.ualberta.ca; web: http://taylor.math.ualberta.ca/~dohan

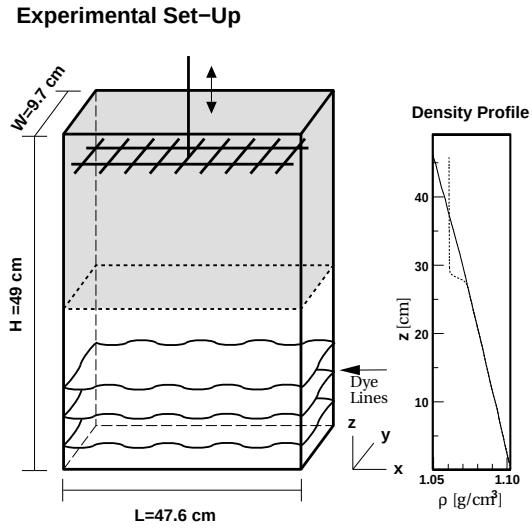

FIGURE 1: The experimental configuration: the tank is filled with uniformly salt-stratified water and a turbulent mixed layer is created at the top (shaded region) of the tank by the oscillating grid. A sample density profile before and after an experiment is included.

A digital camera is positioned a distance $L_{\text{camera}} \approx 4\,\text{m}$ from the tank. The recorded images in the $x-z$ plane are analyzed using the image processing software package, DigImage (Dalziel 1993).

3. EXPERIMENTAL OBSERVATIONS

In all experiments two counter-rotating vortices are established within the turbulent region. The vortices are oriented with rotation vector out of the front of the tank (along the y-axis in Fig. 1) with upwelling at the sides, and downwelling in the centre of the tank. This overall circulation is believed to be a consequence of the high aspect ratio of the tank because turbulent motions with length-scales greater than W are confined to the $x-z$ plane (Dohan and Sutherland 2002). Embedded within these vortices are fast time-scale and small length-scale eddies. The base of the region is deformed by $5-10\,\text{cm}$ wide turbulent jets that push vertically down into the stratified region at random positions along the length of the tank.

Large tank-scale waves are generated below the

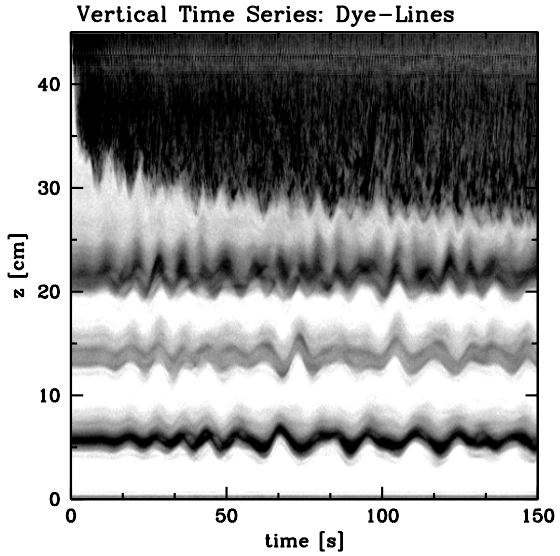

FIGURE 2: A sample false-colour vertical time series image for an experiment with $N = 0.79\,\mathrm{s}^{-1}$. The bottom of the turbulent region is approximately at $z = 28\,\mathrm{cm}$. The vertical motions are tracked by the three dye-lines (dark bands) at isopycnal layers with mean vertical positions 5.4, 12.7 and 20.5 cm above the bottom of the tank.

mixing region within seconds of the start of the experiment. The waves resemble mode 1 or mode 2 (in the horizontal) standing waves in the tank, with mode 2 most frequently observed. Both modes are quasi-two-dimensional, exhibiting negligible variation across the width of the tank. The standing waves are on the scale of the counter-rotating vortices in the turbulence and persist for the duration of the experiments.

Transient wave packets travel down through the three Rhodamine-dyed isopycnal layers. The transient wave packets have horizontal wavelengths on the order of one quarter of the tank length and are observed to be generated from the smaller scale turbulent jets described above.

4. DYE-LINE RESULTS

In the first visualization technique, Rhodamine dye is added to mark three isopycnal layers. A pearlescent dye is distributed across the top of the tank prior to the start of the experiment and marks the spatial extent of the turbulent region.

The time evolution throughout an experiment of the vertical position of the three dye-lines can clearly be seen in a vertical time series, shown in Figure 2 for the first 150 s of an experiment in which $N = 0.79\,\mathrm{s}^{-1}$. The time series is constructed from

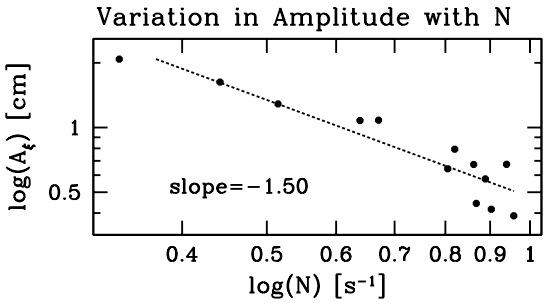

FIGURE 3: The variation in amplitude, A_ξ, of vertical isopycnal fluctuations, ξ, with buoyancy frequency across all experiments. The best-fit line to the logarithmic data is included, and has a slope of -1.50 ± 0.08.

the digitized images of the experiment by storing the pixel column at $x = 29.9\,\mathrm{cm}$ at successive time steps in a single image.

To plot displacement as a function of time at three vertical levels, we fit a contour to the bottom flank of the time series image of each dye-line. Fourier series decompositions of the dye-line contours show that the vertical displacement spectrum is spread throughout the range of allowable wave frequencies $\omega < N$ with peaks that do not correspond to standing waves with either mode 1 or mode 2 in the horizontal and a simple vertical modal structure. The peaks are likely associated with a superposition of modes with comparable amplitudes or with modes having a more complex vertical structure.

Root-mean-square amplitude measurements of the contour lines are shown in Figure 3, plotted against the buoyancy frequency for a range of experiments and on a logarithmic scale. In general, we find a decreasing trend in the amplitude with increasing buoyancy frequency. The slope of the best-fit line to the logarithmic data has a value of -1.50 ± 0.08. Using a variety of averaging techniques, we find that the slopes lie between -1.45 and -1.54, for calculations using all dye-lines and a variety of temporal ranges. This suggests a power law relation of the form

$$A_\xi \sim N^{-1.5} \tag{1}$$

where A_ξ denotes amplitude of the vertical displacement of isopycnal lines.

5. SCHLIEREN RESULTS

The technique of synthetic schlieren (Sutherland et al. 1999) is the second method used to visualize

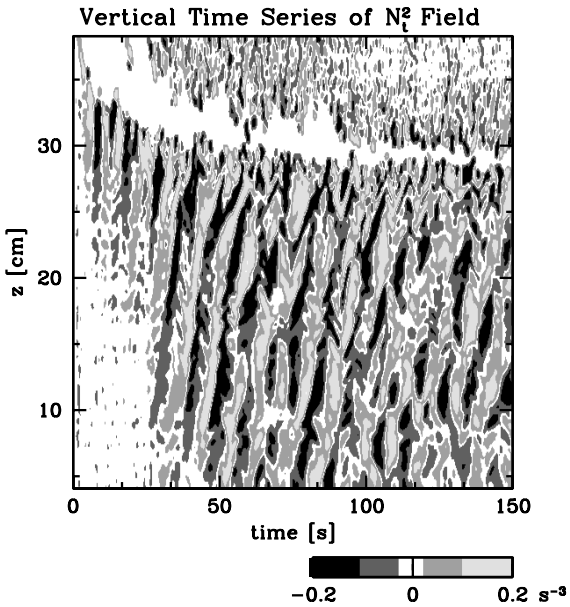

FIGURE 4: A sample vertical time series of an N_t^2 field for an experiment with $N = 1.06$. The horizontal location of the time series is at $x = 36.9$cm from the left side of tank. The bottom of the turbulent region is approximately at $z = 27$cm.

the internal wave field. Schlieren methods are sensitive to density gradients. For convenience, we represent these as the change in buoyancy frequency, and its time derivative, N_t^2. From linear theory, one can derive the basic state fields from the measured N_t^2 field. Wave amplitudes on the order of .001cm can be measured under ideal conditions.

An example of a vertical time series of the N_t^2 field is shown in Figure 4, enhanced with a false colour representation. The base of the turbulent region is traced by the descending white region near the top of the image which extends to approximately 27cm.

In contrast to the dye-line observations, because synthetic schlieren is sensitive to strong local gradients to the background density, the standing waves are not the dominant feature captured by the synthetic schlieren images. The N_t^2 field captures the signal due to turbulent jet-scale downward-propagating waves generated from the base of the turbulent region (the corresponding phase lines move upward in time). The ability to resolve the transient waves from the tank-scale modes throughout the entire wave field is the advantage to the synthetic schlieren technique.

Fourier transforms are used to determine the vertical wavenumbers and frequencies of the internal waves. The most notable feature of the spectra

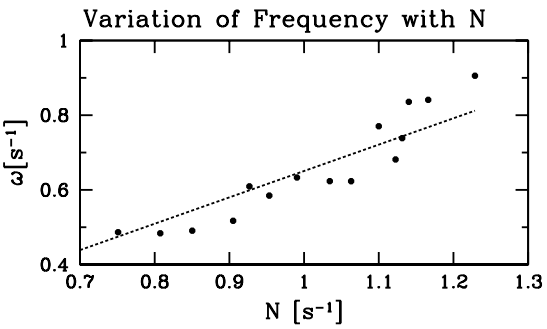

FIGURE 5: The trend in dominant internal wave frequencies with experimental parameter N calculated from the peaks of the Fourier spectra of the N_t^2 fields. The best-fit line to the frequency data and the origin, $(\omega, N) = (0, 0)$ has a slope of 0.71 ± 0.05. This trend corresponds to waves with an angle of propagation to the vertical of $\Theta = 45°$.

of the schlieren time series is that the frequencies and wavenumbers are very localized in wavenumber space. For example, the wavenumbers present in Fig. 4 are grouped around $\omega = 0.58 \pm 0.02\,\mathrm{s}^{-1}$ and $k_z = -0.7 \pm 0.3\,\mathrm{cm}^{-1}$. The peak values for the frequencies over a range of experiments, as calculated from the power spectra analyses, are shown in Figure 5, plotted against N. The measured frequencies follow an increasing linear trend with N.

To measure the amplitudes of the waves in the tank, the rms average of the N_t^2 time series is calculated across $t = 30 - 150$s, to give a profile of average amplitude with depth. The value at the base of the mixed region is chosen as the representative amplitude for each experiment.

The amplitude measurements generally have a decreasing trend. To compare these results for turbulent jet-scale waves with those of tank-scale waves (the dye-line analysis), the slope of the best-fit line to the logarithmic plot of the vertical displacement is taken and suggests a power law relationship of the form $A_\xi \sim N^{-1.68}$.

To illustrate the significance of the vertical displacement amplitude of these waves, in Figure 6 A_ξ is divided by the corresponding horizontal wavelength, λ_x, and plotted against the angle of propagation of the waves with respect to the vertical, Θ. Explicitly, $\Theta = \tan^{-1}(|k_z|/k_x) = \cos^{-1}(\omega/N)$. Included are the critical relative amplitudes for two types of internal wave breaking mechanisms (Sutherland 2001). These are large amplitude waves at approximately one quarter of the amplitude at which they would break.

Surprisingly, we find that across all experiments

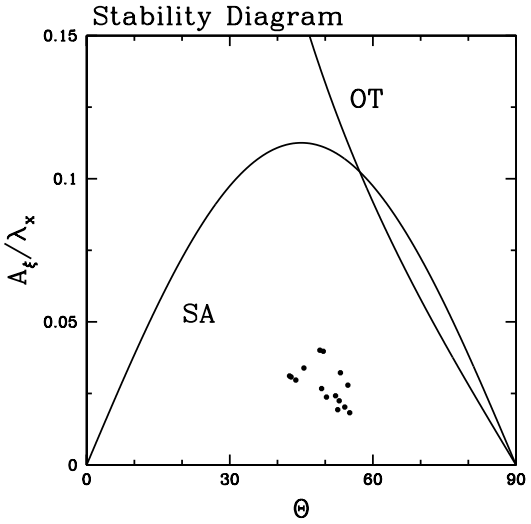

FIGURE 6: The relative amplitudes A_ξ/λ_x of the downward propagating internal waves plotted against their angle of propagation to the vertical, Θ. Included are two critical relative amplitude curves at which waves may break (SA = self-acceleration, OT = overturning).

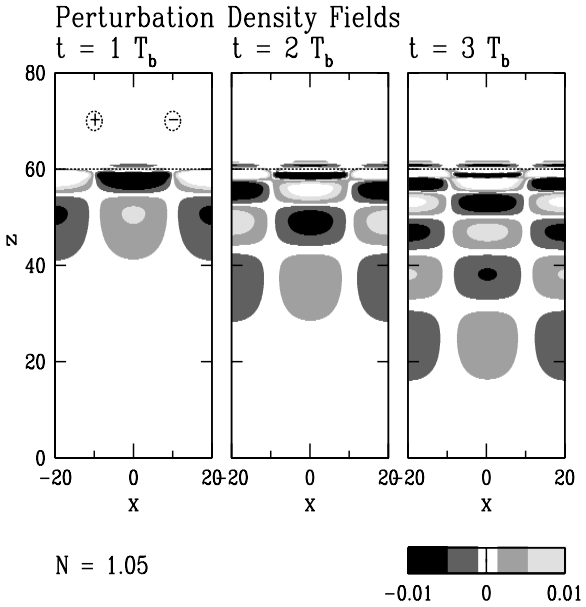

FIGURE 7: Variation of amplitude and vertical wavelength with time: snapshots of the perturbation density fields are shown at 1, 2 and 3 buoyancy periods into a simulation with $N = 1.05$. The structure of the forcing to the vorticity field is superimposed on the mixed region.

the properties of the dominant small-scale waves collapse onto a narrow range of relative amplitude and angles of propagation. The angles of wave propagation to the vertical all lie within $\Theta = 42° - 55°$, with an average value of 50°. Thus, although turbulent eddies can excite a broad frequency spectrum, the largest amplitude waves have a frequency that is an approximately constant function of N.

6. NUMERICAL SIMULATIONS

Internal wave generation from a mixed region is further examined using a fully nonlinear numerical model in two dimensions that simulates a uniformly stratified Boussinesq fluid underlying a homogeneous mixed region. The domain is horizontally periodic with free-slip upper and lower boundaries.

The prognostic equations for vorticity and perturbation density are given by:

$$\frac{\partial \omega}{\partial t} + \mathbf{u}\cdot\nabla\omega = \frac{g}{\rho_0}\frac{\partial \rho}{\partial x} + \nu\nabla^2\omega + \mathcal{F}_\omega \qquad (2)$$

$$\frac{\partial \rho}{\partial t} + \mathbf{u}\cdot\nabla\rho + w\frac{d\overline{\rho}}{dz} = \kappa\nabla^2\rho \qquad (3)$$

where ν is the kinematic viscosity, κ is the thermal diffusivity, and the background hydrostatic density field, $\overline{\rho}$, has been subtracted from the equations.

The mixed layer is simulated by a homogeneous top layer that overlies a uniformly stratified region. The initial stratification is given by:

$$N = \begin{cases} N_0^2 & 0 < z < 60 \\ 0 & 60 < z < 80. \end{cases}$$

Since we are interested in the internal waves, the time-scales of turbulence cannot be resolved with our simulations. Rather, the mixed region is superimposed with a vorticity field. Motivated by the circulations observed in the laboratory experiments, two counter-rotating vortices are forced in the mixed region:

$$\mathcal{F}_\omega = 0.1e^{(-\frac{1}{2}(\frac{(x+10)^2}{4}+\frac{(z-70)^2}{4}))} + -0.1e^{(-\frac{1}{2}(\frac{(x-10)^2}{4}+\frac{(z-70)^2}{4}))}.$$

The evolution of the vertical structure of the wave field over time is evident in Figure 7, which shows the perturbation density field of a simulation with $N = 1.05$ at one, two and three buoyancy periods into the simulation. In these simulations, perturbation density is scaled with nondimensional vertical displacement. Since the vorticity field is constantly being forced throughout these simulations, the amplitudes of the internal waves do not reach steady state and grow in time.

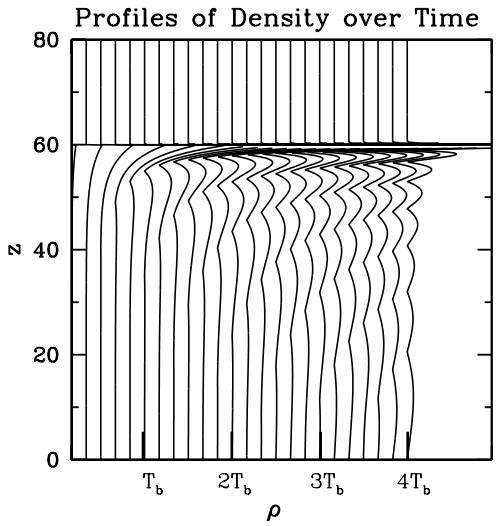

FIGURE 8: Profiles of amplitude of perturbation density field (averaged across the horizontal domain) over 4 buoyancy periods.

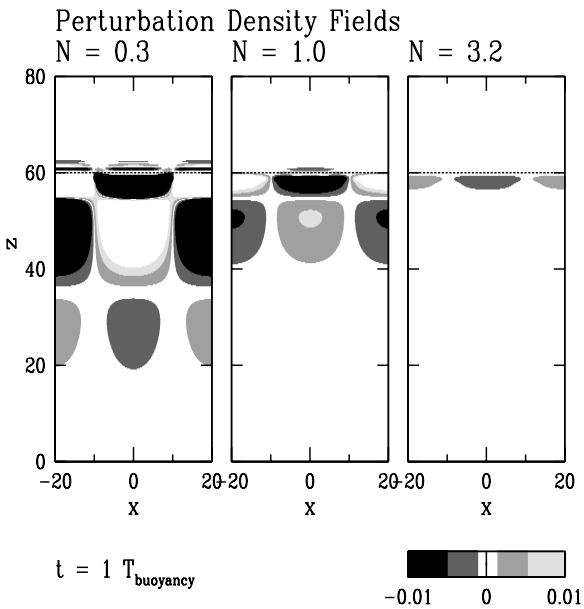

FIGURE 9: Qualitative variation of amplitude of perturbation density field with buoyancy frequency. All plots are calculated one buoyancy period into the simulation.

The density field shows the presence of waves with the same structure as the large-scale waves observed in the experiments. The waves have the same mode 2 structure in the horizontal, but with a much richer vertical structure than the first simplest mode of the tank. The dispersive nature of the wave field can be seen by the change in vertical wavelength of the wave field over time.

Another visualization of the wave field over time is shown in Figure 8, which plots vertical profiles of the average amplitude across the horizontal domain of the perturbation density field. The profiles are plotted at successive times over four buoyancy periods. In this image, the group velocity of the downward propagating wave packet is seen by the envelope of the perturbations to the background density, while the phase lines of the waves are seen to travel upwards in time.

If the stratification is varied, the amplitudes of the waves show a consistent variation with buoyancy frequency as that seen in the experiments. Qualitatively this decrease in amplitude with an increase in buoyancy frequency can be seen in Figure 9 which plots the perturbation density fields for simulations with three values of N.

Figure 10 plots the temporal variation in wave amplitude with stratification. The characteristic amplitude for each experiment is chosen as the amplitude at a fixed location, $z = 55$, averaged over one buoyancy period. Since the vorticity is continually forced, the average amplitude of the waves at a fixed position grows in time and is observed to follow $A \sim t^{0.46}$, shown in Fig. 10a). The total variation in amplitude with both stratification and time is shown in Fig. 10b) and is observed to follow $A \sim N^{-1.97}$. By averaging over one buoyancy period, and assuming a power-law relation of amplitude with time, the steady-state variation of amplitude with stratification is then $A_{\text{steady state}} \sim N^{-1.97+0.46}$. Therefore,

$$A_\xi \sim N^{-1.51}. \tag{4}$$

7. DISCUSSION AND CONCLUSIONS

Dye-line and schlieren analyses reveal two scales of internal wave motions in the laboratory experiments. The large-scale motions have a modal (tank-scale) structure and small-scale transient wavepacket bursts are observed on the scale of the turbulent jets. These results suggest that there are two mechanisms for generating internal waves from the turbulence in our experimental situation: the two counter-rotating vortices in the turbulence and the "bursts" of turbulent jets that break into the stratified region.

Although a range of frequencies may potentially be excited by the turbulence, the wave spectra of the downward-propagating eddy-scale waves exhibit a common narrow frequency range across all

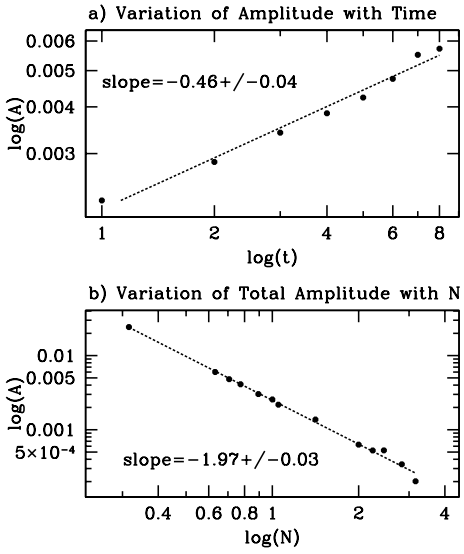

FIGURE 10: a) Variation of amplitude of wave field with time for a simulation with $N = 1.05$. b)Variation of total amplitude of wave field with buoyancy frequency, N. The total amplitude variation is the sum of the varition with time and the variation with stratification.

experiments.

There are two possible explanations: instability and resonance. Waves with angles of 45° can have the largest relative amplitudes before becoming unstable. Because the observed amplitudes are approximately 25 percent of that required for breaking, this explanation seems unlikely.

It is more likely that the waves are excited through resonant feedback with the turbulence. For example, consider the vertical flux of horizontal momentum, given by the Reynolds stress $\rho_0\langle uw\rangle$, which can be written for small-amplitude waves in terms of A_ξ by

$$\rho_0\langle uw\rangle = \frac{1}{4}\rho_0 N^2 A_\xi^2 \sin(2\Theta). \qquad (5)$$

The maximum transport by internal waves occurs when $\Theta = 45°$. Likewise, the vertical energy flux per unit horizontal area carried by waves of amplitude A_ξ can be expressed by

$$F_z = \frac{1}{2}\frac{\rho_0 A_\xi^2 N^3}{k_x}\sin\Theta\cos^2\Theta. \qquad (6)$$

The maximum vertical energy flux occurs for $\Theta = 35°$, the angle at which the vertical group velocity is greatest. Since waves transport energy and momentum away from the turbulent region, waves with Θ in the range $35° - 45°$ may act most efficiently to modify the turbulence in a way that enhances their excitation.

The amplitudes of both the large- and small-scale internal waves are observed to scale with buoyancy frequency as $A_\xi \sim N^{-p}$ with $p = 1.50$ for large-scale waves and $p = 1.68$ for small-scale waves. This power law scaling can largely be explained if we assume that the vertical energy flux, given by (6), is constant in all experiments, in which case $A_\xi \sim N^{-3/2}$.

The wave properties in the numerical simulations are qualitatively similar to the waves observed in the experiments and show the same dependence of wave amplitude with stratification as $A \sim N^{-3/2}$.

These preliminary numerical results suggest that a large part of the dynamics of the interaction between internal waves and turbulent mixed regions may be captured in this simple model.

References

Dalziel, S. B. 1993. Rayleigh-Taylor instability: Experiments with image analysis. *Dyn. Atmos. Oceans*, 20:127–153.

Dohan, K. and Sutherland, B. R. 2002. Turbulence time-scales in mixing box experiments. *Expt. Fluids*, 33:709–719.

Dohan, K. and Sutherland, B. R. 2003. Internal waves generated from a turbulent mixed region. *Phys. Fluids*, 15:488–498.

Sutherland, B. R. 2001. Finite-amplitude internal wavepacket dispersion and breaking. *J. Fluid Mech.*, 429:343–380.

Sutherland, B. R., Dalziel, S. B., Hughes, G. O., and Linden, P. F. 1999. Visualisation and measurement of internal waves by "synthetic schlieren". Part 1: Vertically oscillating cylinder. *J. Fluid Mech.*, 390:93–126.